

# NMR Structure and Metal Interactions of the CopZ Copper Chaperone\*

(Received for publication, March 30, 1999)

Reinhard Wimmer<sup>‡§</sup>, Torsten Herrmann<sup>‡</sup>, Marc Solioz<sup>¶||</sup>, and Kurt Wüthrich<sup>‡</sup>

From the <sup>‡</sup>Institute of Molecular Biology and Biophysics, ETH Hönggerberg, CH-8093 Zurich, Switzerland and the <sup>¶</sup>Department of Clinical Pharmacology, University of Berne, CH-3010 Berne, Switzerland

**A recently discovered family of proteins that function as copper chaperones route copper to proteins that either require it for their function or are involved in its transport. In *Enterococcus hirae* the copper chaperone function is performed by the 8-kDa protein CopZ. This paper describes the NMR structure of apo-CopZ, obtained using uniformly <sup>15</sup>N-labeled CopZ overexpressed in *Escherichia coli* and NMR studies of the impact of Cu(I) binding on the CopZ structure. The protein has a  $\beta\alpha\beta\beta\alpha\beta$  fold, where the four  $\beta$ -strands form an antiparallel twisted  $\beta$ -sheet, and the two helices are located on the same side of the  $\beta$ -sheet. A sequence motif GMX-CXXC in the loop between the first  $\beta$ -strand and the first  $\alpha$ -helix contains the primary ligands, which bind copper(I). Binding of copper(I) caused major structural changes in this molecular region, as manifested by the fact that most NMR signals of the loop and the N-terminal part of the first helix were broadened beyond detection. This effect was strictly localized, because the remainder of the apo-CopZ structure was maintained after addition of Cu(I). NMR relaxation data showed a decreased correlation time of overall molecular tumbling for Cu(I)-CopZ when compared with apo-CopZ, indicating aggregation of Cu(I)-CopZ. The structure of CopZ is the first three-dimensional structure of a cupro-protein for which the metal ion is an exchangeable substrate rather than an integral part of the structure. Implications of the present structural work for the *in vivo* function of CopZ are discussed, whereby it is of special interest that the distribution of charged residues on the CopZ surface is highly uneven and suggests preferred recognition sites for other proteins that might be involved in copper transfer.**

Two key elements of copper homeostasis are the CPx-type heavy metal ATPases, which transport copper across cell membranes (1, 2), and the copper chaperones, which mediate intracellular copper transport (3, 4). This paper describes studies of

the CopZ copper chaperone of *Enterococcus hirae*, which belongs to a family of small 8-kDa proteins that are highly conserved between species. CopZ is encoded by the cop-operon (5–7), which appears to be both essential and sufficient for copper homeostasis in this organism. It encodes, in addition to CopZ, a copper import and a copper export CPx-type ATPase, CopA and CopB, respectively, and a copper-responsive repressor, CopY. CopZ has recently been shown to donate copper(I) to CopY *in vitro* (8).

Copper chaperones homologous to CopZ have also been described for yeast (Atx1), plants (CCH), and humans (HAH1) (3, 9, 10). A related bacterial protein, MerP, has a similar role in mercury transport (11). All these proteins possess the putative metal-binding site GMXCXXC, suggesting a universal mechanism of metal binding and transfer. The CXXC motif and other sequence features of heavy metal chaperones are also present in the N-terminal domains of CPx-type copper and cadmium ATPases (12), in the N-terminal domains of mercuric reductases (13), and, in multiple copies, in metallothioneins (14). Typically, one or two such motifs are present in bacterial and yeast proteins (15), whereas up to six closely similar motifs are present in mammalian copper ATPases (2, 16). Involvement of the cysteine residues of the conserved GMXCXXC motif in metal ion binding of MerP and cadmium ATPase suggested by mutational analysis (11, 17, 18) was directly evidenced by the NMR solution structure of the bacterial mercury chaperone, MerP, and the fourth chaperone-like metal-binding domain of the Menkes copper ATPase, MNKr4 (19, 20). However, MerP binds mercury(II), which has different coordination properties from those of copper(I), and the structure of MNKr4 was determined with bound silver(I), which is not the natural ligand of this protein. In this paper, to gain further insight into the structural basis of the function of copper chaperones, we solved the NMR structure of apo-CopZ and investigated the effects of Cu(I) binding on the structure of CopZ with a variety of NMR techniques.

## EXPERIMENTAL PROCEDURES

**CopZ Overexpression and Purification**—The *copZ* gene was amplified with the polymerase chain reaction, using TaqPlus (Stratagene, Inc.) and the primers 5'-gaaacaacctggcacaagaattt and 5'-acatgtcactgcagatagatacaaa. The product was cut with *Nco*I and *Pst*I and ligated into pQE6 (Qiagen), cut with *Pst*I and partially cut with *Nco*I. The final construct, pDZ69, was verified by DNA sequencing. CopZ was overexpressed from pDZ69 in *Escherichia coli* BL21 (Stratagene), which was grown aerobically in a 10 liter fermenter at 35 °C using M9 medium, supplemented with 10  $\mu$ g/ml of thiamin and containing 0.05% <sup>15</sup>NH<sub>4</sub>Cl as the sole nitrogen source. Cells were induced and extracts prepared as described (21). The extracts were diluted with an equal volume of water, made 10 mM in dithiothreitol, filtered through a Whatman cellulose filter, and loaded onto a 3  $\times$  14-cm S-Sepharose column. CopZ was eluted with a 0–300 mM K<sub>2</sub>SO<sub>4</sub> gradient in buffer A (50 mM Tris-SO<sub>4</sub> at pH 7.4, 10 mM dithiothreitol). The CopZ fractions were pooled and concentrated to less than 5 ml with an Amicon YM3 membrane. Final purification was achieved by gel filtration on a 2  $\times$  60-cm TSK G3000

\* This work was supported by Grant 3200-046804 from the Swiss National Foundation and Grant 3392.1 from the Kommission für Technologie und Innovation (KTI). The costs of publication of this article were defrayed in part by the payment of page charges. This article must therefore be hereby marked "advertisement" in accordance with 18 U.S.C. Section 1734 solely to indicate this fact.

The atomic coordinates and structure factors (code lcpz) have been deposited in the Protein Data Bank, Research Collaboratory for Structural Bioinformatics, Rutgers University, New Brunswick, NJ (<http://www.rcsb.org/>). The chemical shifts were deposited in the BioMagResBank (accession code 4344).

§ Recipient of Grant J1559-GEN from the Fonds zur Förderung der wissenschaftlichen Forschung (Austrian Science Fund).

|| To whom correspondence should be addressed: Dept. of Clinical Pharmacology, University of Berne, Murtenstrasse 35, 3010 Berne, Switzerland. Tel.: 41-31-632-3268; Fax: 41-31-632-4997; E-mail: marc.solioz@ikp.unibe.ch.

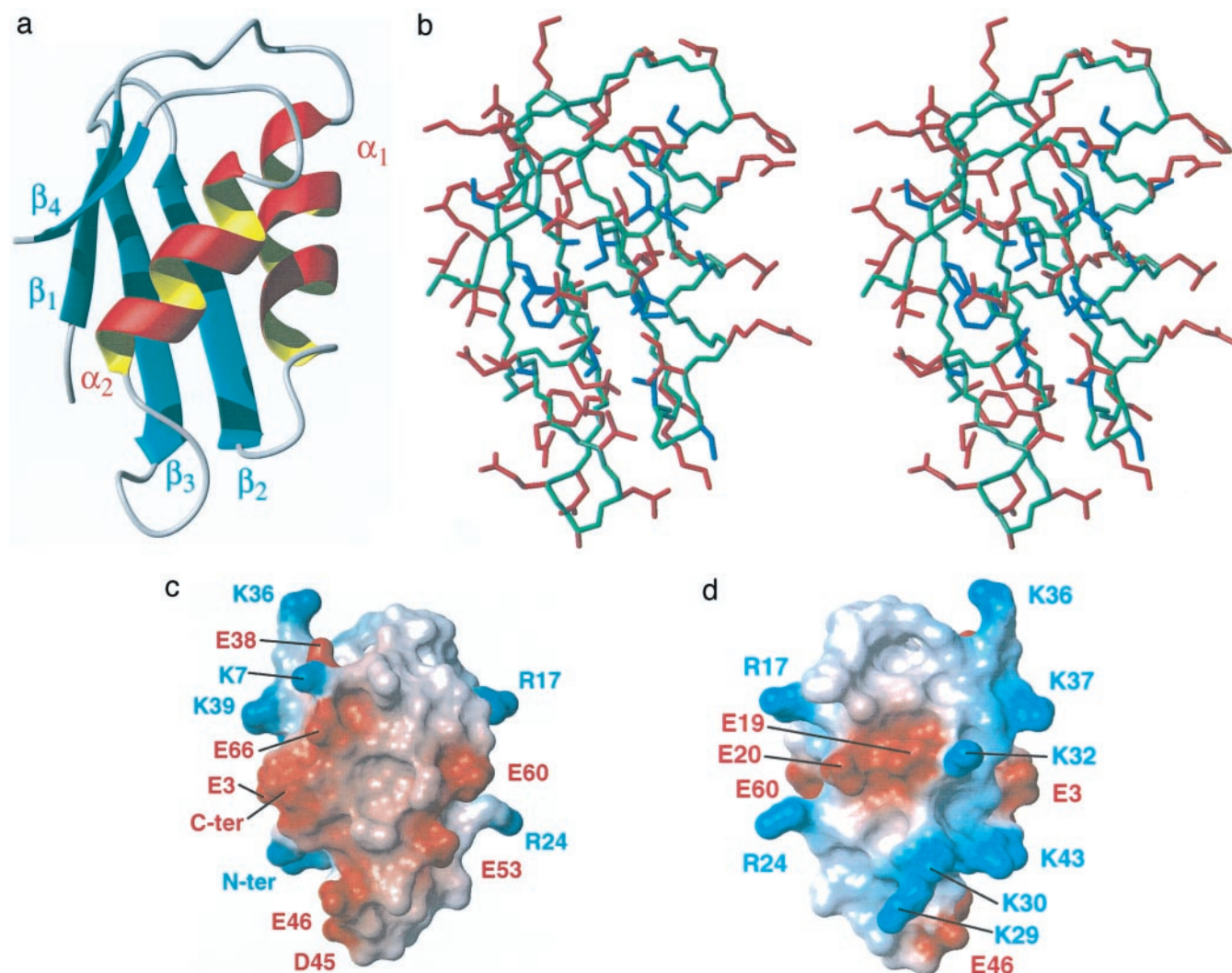


**FIG. 1. The NMR structure of apo-CopZ.** Panel a, ribbon-drawing of the apo-CopZ conformer with the lowest residual DYANA target function value. The regular secondary structure elements are  $\alpha_1$  (14–24) and  $\alpha_2$  (51–59) in red and yellow, and  $\beta_1$  (2–7),  $\beta_2$  (28–34),  $\beta_3$  (39–44), and  $\beta_4$  (64–67) in blue. This figure and all other structure models were prepared with the program MOLMOL (46). Panel b, stereo view of an all-heavy atom presentation of apo-CopZ in the same orientation as in panel a. The backbone is drawn in green, the best-defined side chains with an average global heavy atom displacement below 0.6 Å in blue, and the other side chains in red. Panels c and d, surface electrostatic potential distribution of apo-CopZ. The view in panel c was obtained starting with the view in panel a through subsequent counterclockwise rotations by 20° about a horizontal axis and by 30° about a vertical axis; panel d was generated from panel c by a 180° rotation about a vertical axis. Red denotes negatively charged regions, blue denotes positively charged regions. In panels c and d the residues are indicated that account for the electrostatic surface potential.

column (TosoHaas) in buffer A. CopZ was finally concentrated by absorption on a 1 × 5-cm S-Sepharose column, followed by elution with buffer B (50 mM Tris-SO<sub>4</sub> at pH 7.4, 300 mM K<sub>2</sub>SO<sub>4</sub>, 100 mM dithiothreitol). If necessary, these fractions were further concentrated with Millipore Ultrafree-15 centrifugal concentrators. The final CopZ fractions were stored under argon at –20 °C. The purity was greater than 95% as assessed by electrospray mass spectroscopy, amino acid analysis, and gel electrophoresis/silver staining. The N-terminal sequence of CopZ isolated from *E. coli* was AQ instead of MKQ as predicted from the gene sequence. When CopZ was expressed from the same plasmid in *E. hirae*, it had the expected N-terminal sequence MKQ. The reason for this disparity is currently under investigation. The amino acid numbering used in this work corresponds to CopZ with the truncated AQ N terminus.

**Preparation of CopZ NMR Samples**—Purified CopZ at a concentration of at least 10 mg/ml was dialyzed twice for 2 h against 250 volumes of buffer C (50 mM sodium phosphate, 10 μM Na<sub>2</sub>S<sub>2</sub>O<sub>4</sub>, pH 7) in an anaerobic hood at room temperature. To prepare copper(I)-loaded CopZ, the protein was similarly dialyzed under anaerobic conditions twice for 2 h against buffer D (50 mM sodium phosphate, 10 μM Na<sub>2</sub>S<sub>2</sub>O<sub>4</sub>, pH 7, 2% deuterated acetonitrile) and once for 1.5 h against buffer D containing 100 μM [Cu(I)(CH<sub>3</sub>CN)<sub>2</sub>]ClO<sub>4</sub>. Dialyzed CopZ samples were filtered, supplemented with 5% D<sub>2</sub>O, and sealed anaerobically

in NMR tubes. The concentration of apo-CopZ was 1.3 mM and that of Cu(I)CopZ was 0.7 mM. Higher concentrations of Cu(I)CopZ could not be maintained in solution. The samples were stable for several months at 15 °C.

**NMR Spectroscopy and NMR Structure Calculation**—NMR spectra were acquired on BRUKER DRX500, DRX600, and DRX750 spectrometers equipped with (<sup>1</sup>H/<sup>13</sup>C/<sup>15</sup>N) triple resonance probes with pulsed field gradients. All NMR spectra were recorded at 288 K (apo-CopZ is unstable at higher temperatures). The NMR data were processed with the XWinNMR software and the spectral analysis was done with XEASY (22). Homonuclear two-dimensional 2QF-COSY,<sup>1</sup> 3QF-COSY, TOCSY (50 and 90 ms mixing time), and NOESY (50 ms mixing time) spectra as well as three-dimensional <sup>15</sup>N-resolved [<sup>1</sup>H,<sup>1</sup>H] TOCSY (mixing time, 50 ms) and <sup>15</sup>N-resolved NOESY (mixing time 50 ms) spectra were used to obtain the sequential assignments (23). Side chain resonances were assigned using two-dimensional 2QF-, 3QF-COSY (24, 25), and TOCSY spectra. A natural abundance [<sup>13</sup>C,<sup>1</sup>H]-COSY spectrum

<sup>1</sup> The abbreviations used are: 2QF-COSY, double quantum filtered correlation spectroscopy; 3QF-COSY, triple quantum filtered COSY; NOE, nuclear Overhauser effect; NOESY, NOE spectroscopy; TOCSY, total correlation spectroscopy; r.m.s.d., root mean square deviation.

TABLE I

Characterization of the energy-minimized NMR structure of apo-CopZ

NMR spectra were recorded with an aqueous solution containing 1.3 mM of CopZ, pH 7, T = 15 °C. The input for the structure calculation consisted of 993 NOE upper distance limits (201 intrareidual, 277 sequential, 218 medium range, 297 long range) and 323 dihedral angle constraints (97 for  $\phi$ , 73 for  $\psi$ , 100 for  $\chi^1$ , 53 for  $\chi^2$ ). The average residual target function value for the 20 best DYANA conformers before energy minimization was  $1.67 \pm 0.30$  Å.

Quantity	20 Conformers <sup>a</sup>
Residual distance constraint violations	
Number $\geq 0.1$ Å	$1.7 \pm 1.3$
Maximum (Å)	$0.11 \pm 0.01$
Residual dihedral angle constraint violations	
Number $\geq 2.5$ °	$3.0 \pm 2.0$
Maximum (°)	$5.85 \pm 0.01$
AMBER energies (kcal mol <sup>-1</sup> )	
Total	$-2374 \pm 93$
van der Waals	$-187 \pm 10$
Electrostatic	$-2717 \pm 99$
R.m.s.d. from ideal geometry	
Bond lengths (Å)	$0.0076 \pm 0.0002$
Bond angles (°)	$2.13 \pm 0.05$
Peptide bonds (°)	$8.1 \pm 0.6$
R.m.s.d. to the average coordinates <sup>b</sup> (Å)	
N,C $^{\alpha}$ ,C' (2–67)	$0.46 \pm 0.05$
N,C $^{\alpha}$ ,C' (2–7, 14–24, 28–34, 39–45, 50–59, 64–67) <sup>c</sup>	$0.32 \pm 0.06$
Heavy atoms (2–67)	$0.94 \pm 0.06$
Heavy atoms (2–7, 14–24, 28–34, 39–45, 50–59, 64–67) <sup>c</sup>	$0.85 \pm 0.08$

<sup>a</sup> For each entry the average for the 20 energy-refined conformers with the lowest residual DYANA target function values and the variation among the 20 conformers are given.

<sup>b</sup> Average coordinates of the 20 energy-minimized conformers after superposition for best fit of the N, C $^{\alpha}$ , and C' atoms of the residues indicated in parentheses.

<sup>c</sup> These are all the regular secondary structures in apo-CopZ.

was used to obtain the assignment of the methionine-H $^{\epsilon}$  and of some isoleucine side chains. For apo-CopZ, all carbon-bound protons and the backbone and side chain, amide protons have been assigned, except for Ala-1 H $^N$ , His-13 H $^N$ , and Lys-36 H $^{\gamma}$ , H $^{\delta}$  and H $^{\epsilon}$  (all resonances of Lys-36 were very weak), Gln-2 H $^{\beta}$  and H $^{\gamma}$ , Lys-7 H $^{\gamma}$  and H $^{\delta}$ , and Glu-60 H $^{\beta}$  and H $^{\gamma}$ . Of the exchangeable protons only Cys-55 H $^{\gamma}$  could be observed and assigned. Of the Cu(I) form, only a few protons from residues 11–20 were observed. Outside this region most carbon-bound protons could be assigned. The assignments were deposited in the BioMagResBank.

<sup>3</sup>J<sub>HNC $\alpha$</sub>  coupling constants were obtained from a [<sup>15</sup>N,<sup>1</sup>H]-COSY spectrum using the INFIT procedure (26). <sup>3</sup>J<sub>N $\beta$</sub>  coupling constants were measured using the three-dimensional constant time-HNNHB experiment (27). <sup>15</sup>N(<sup>1</sup>H) heteronuclear NOEs were determined by comparing volumes of cross peaks in [<sup>15</sup>N,<sup>1</sup>H]-COSY spectra with and without proton saturation during the relaxation delay (28), T<sub>1</sub> and T<sub>2</sub> relaxation times of <sup>15</sup>N were obtained by exponential fitting of peak intensities in [<sup>15</sup>N,<sup>1</sup>H]-COSY spectra acquired with different relaxation delays (28). Sample spinning to avoid convection effects (29) was found to considerably improve the quality of the relaxation data recorded at 500 MHz.

Cross-peak volumes of NOESY spectra were converted to distance constraints using the subroutine CALIBA (30) in DYANA (31). For the apo form, a total of 1,258 <sup>1</sup>H-<sup>1</sup>H NOEs and 133 coupling constants could be obtained. These were converted into the distance and torsion angle constraints listed in Table I, using data processing with the DYANA subroutine FOUND (32). The final round of structure calculations with DYANA was started with 50 random structures, and the 20 conformers with the lowest residual target function values were energy minimized using the program OPAL (33).

**Miscellaneous Methods**—The synthesis of diacetonitrilo-copper(I) perchlorate, [Cu(I)(CH<sub>3</sub>CN)<sub>2</sub>]ClO<sub>4</sub>, was performed as described (34). Protein concentrations were determined by quantitative amino acid analysis, and copper concentrations were determined by flame atomic absorption spectroscopy, using a Varian A-8875 instrument. Electron paramagnetic resonance (EPR) spectra were recorded at 77 K on a BRUKER ESP 300 CW-spectrometer. The resonance frequency was 9.416 GHz, and the field was swept from 2,500 to 3,900 G. The mass of unlabeled and uniformly <sup>15</sup>N-labeled apo-CopZ was determined on a VG platform single quadrupole mass spectrometer (Micromass, Manches-

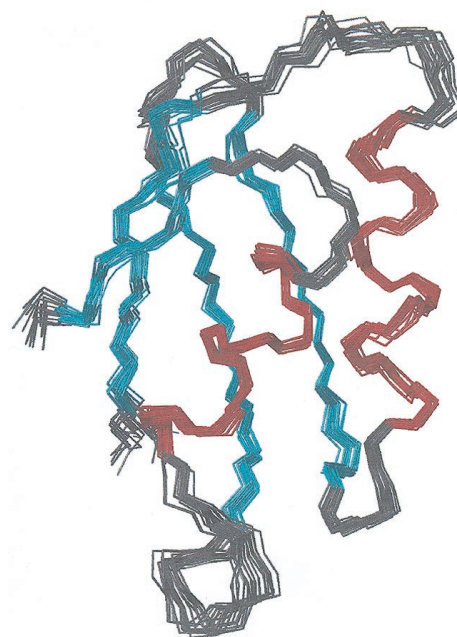


FIG. 2. Bundle of the 20 best energy-refined conformers of apo-CopZ.  $\beta$ -sheet regions are colored blue and  $\alpha$ -helices are red. The orientation of the molecule is the same as in Fig. 1a.

ter, UK), using an atmospheric pressure electrospray ion source with an upper mass limit of  $m/z$  3,000 in 50% acetonitrile, 1% formic acid. N-terminal amino acid sequencing was performed with an Applied Biosystems 477A protein sequencer. Light scattering measurements were conducted on a "DynaPro 801" photometer from ProteinSolutions at 900 Å; the detector was oriented at 90° relative to the excitation beam. The samples were filtered under nitrogen through a 20-nm mesh and measured immediately.

## RESULTS

**NMR Structure of apo-CopZ**—The polypeptide fold of apo-CopZ consists of a strongly twisted four-stranded antiparallel  $\beta$ -sheet and two  $\alpha$ -helices that are both located on the same side of the  $\beta$ -sheet (Fig. 1a). The axes of the two helices are at an angle of about 45°.  $\alpha_1$  runs approximately parallel to  $\beta_2$  and  $\beta_3$ , whereas  $\alpha_2$  is aligned parallel to  $\beta_1$  and  $\beta_4$ . The two presumed copper binding residues, Cys-11 and Cys-14, are located in a loop between  $\beta_1$  and  $\alpha_1$ , and Cys-14 is actually the first residue of  $\alpha_1$ . The amino acid side chains form a well ordered core with 19 residues having smaller average global displacements than 0.6 Å (Fig. 1b). The cysteines 11 and 14 of the CXXC motif, which form the core of the metal-binding site, adopt conformations that do not represent a pre-formed copper-binding site, so that metal binding will require major side chain structural rearrangement. The surface side chains form a remarkably uneven distribution of positive and negative charges; Glu-3, and the five Asp and Glu residues in the peptide segment 45–66, and the C-terminal carboxylate form a large negative surface patch (see Fig. 1c). On the opposite surface relative to the aforementioned negative patch, a ring of positive charges is formed by 6 Lys residues in the segment 29–39 and the 2 arginines of helix  $\alpha_1$ .

As can be seen from Table I, the structure of apo-CopZ is very well defined. For the secondary structure elements a r.m.s.d. of 0.32 Å was calculated for the backbone heavy atoms, and when the somewhat less well ordered regions 35–38 and 8–13 were included, the r.m.s.d. increased to 0.46 Å. The high precision of the structure determination is clearly reflected in the bundle of 20 best conformers shown in Fig. 2. Fig. 3a shows that there is a high density of medium range NOEs in the two helical regions, and the  $\beta$ -sheet topology is well supported by numerous

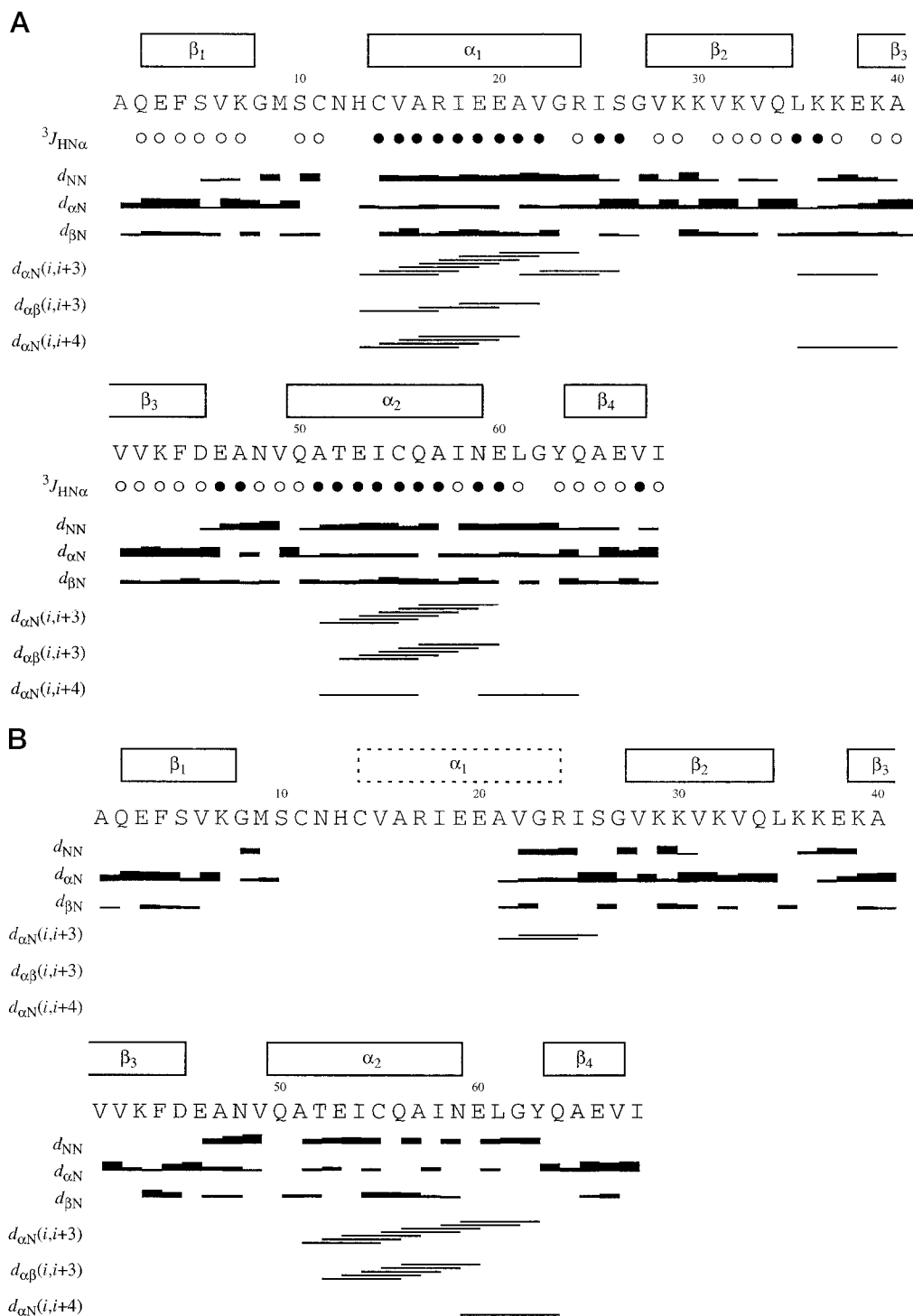


**FIG. 3. Amino acid sequence of CopZ with survey of the sequential connectivities and additional data collected for secondary structure identification.** *a*, apo-CopZ; *b*, Cu(I)-CopZ. The sequential NOE connectivities  $d_{\alpha N}$ ,  $d_{NN}$ , and  $d_{\beta N}$  are indicated by black bars of a thickness that corresponds to the strength of the NOEs. The medium range connectivities  $d_{\alpha N}(i, i + 3)$  and  $d_{\alpha\beta}(i, i + 3)$  are shown by lines starting and ending at the positions of the residues related by the NOE. In the row  ${}^3J_{HN\alpha}$ , filled and open circles denote residues with  ${}^3J_{HN\alpha} < 6$  Hz and  ${}^3J_{HN\alpha} > 7$  Hz, respectively. The sequence locations of secondary structure elements are given at the top, where the dotted box in Cu(I)-CopZ represents the helix  $\alpha_1$  in apo-CopZ.

interstrand NOEs (Fig. 4). 83% of the  $(\phi, \psi)$ -pairs in apo-CopZ were found to be within the most favored regions of the Ramachandran plot and 13% within the additionally allowed regions (calculated with PROCHECK-NMR, Ref. 35).

**Structure Rearrangement upon Interaction of apo-CopZ with Cu(I)**—Throughout the entire  $\beta$ -sheet and the helix  $\alpha_2$  there are only small changes in backbone chemical shifts upon interaction of apo-CopZ with Cu(I) (Fig. 5), which indicates that no

major structural changes of the backbone took place in these regions. A larger impact of the addition of Cu(I) is seen in the polypeptide segment 9–22, which is either manifested by larger chemical shift variations or, for the residues 11–20, by the fact that most NMR signals could not be observed after addition of Cu(I), possibly because of line-broadening due to conformational exchange processes. In any case, a strong impact of Cu(I) addition on the apo-CopZ structure is primarily restricted to

FIG. 4. Interstrand NOEs defining the  $\beta$ -sheet topology in *apo*-CopZ. Each double-headed arrow identifies an experimental NOE constraint. Several anticipated  $H^{\alpha}$ - $H^{\alpha}$  NOEs could not be observed because of overlap with the water signal. The hydrogen bonds are indicated by wavy lines.

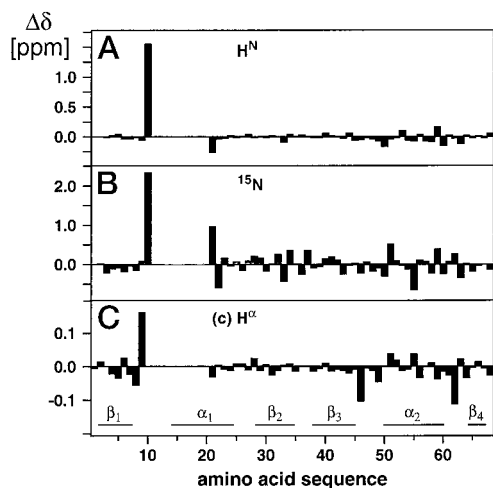
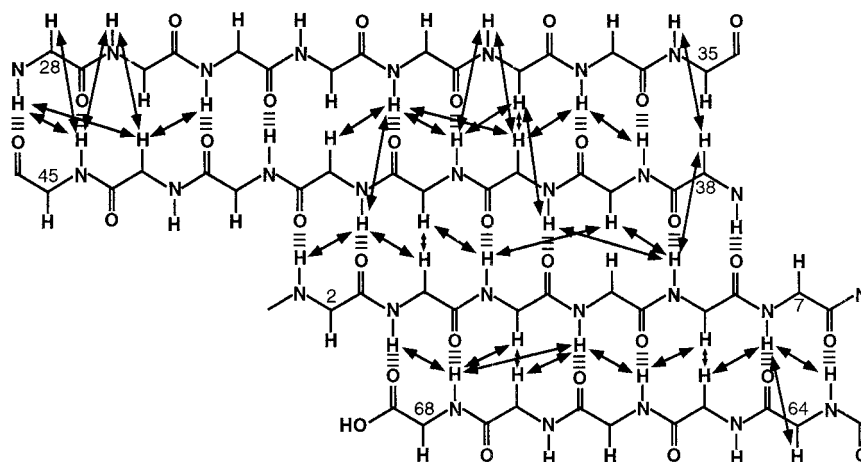


FIG. 5. Differences between corresponding backbone chemical shifts in *apo*-CopZ and Cu(I)-CopZ plotted versus the sequence. Amide protons  $\Delta\delta(H^N)$  (a), amide nitrogens  $\Delta\delta(^{15}N)$  (b),  $\alpha$ -protons  $\Delta\delta(H^{\alpha})$  (c) (in the case of glycines, the pair of  $H^{\alpha}$  lines with the biggest difference was chosen), where  $\Delta\delta = \delta(\text{apo-CopZ}) - \delta(\text{Cu(I)-CopZ})$ .

the residues 9–22, which include the presumed Cu(I) ligands (11, 17, 18). Outside this segment there is one outstanding  $H^{\alpha}$  chemical shift change in each of the two loops that connect the helix  $\alpha_2$  with the  $\beta$ -sheet.

To obtain additional data that could be used to further characterize possible dynamic processes implicated by the disappearance of most  $^1H$  NMR lines for the residues 11–20, the relaxation times  $T_1$  and  $T_2$  of  $^{15}N$  and the  $^{15}N\{^1H\}$ -NOEs of both *apo*-CopZ and Cu(I)-CopZ were measured. Plots of the relaxation data versus the sequence (Fig. 6) show that the  $T_1$  values throughout the structured part of the protein were significantly longer for Cu(I)-CopZ than for *apo*-CopZ, whereas the  $T_2$  values were significantly shorter for Cu(I)-CopZ. For the structured part of the protein the increase of the  $T_1/T_2$  ratio is a direct measure for decreased overall rotational tumbling of the molecule. The average  $T_1/T_2$  ratio for *apo*-CopZ was  $3.7 \pm 0.2$ , which for a spherical particle corresponds to an overall rotational correlation time of  $\tau_c = 6.2 \pm 0.3$  ns (36), whereas for Cu(I)-CopZ the average  $T_1/T_2$  ratio of  $8.1 \pm 0.9$  corresponds to a  $\tau_c = 10.2 \pm 0.6$  ns. The observed increase of the rotational correlation time of Cu(I)-CopZ when compared with *apo*-CopZ, and the concomitant reduced overall mobility are indicative of self-aggregation of Cu(I)-CopZ. The  $^{15}N\{^1H\}$ -NOEs do not indicate any region of high backbone flexibility other than the N termini and possibly the vicinity of the copper-binding sites in both *apo*-CopZ and Cu(I)-CopZ.

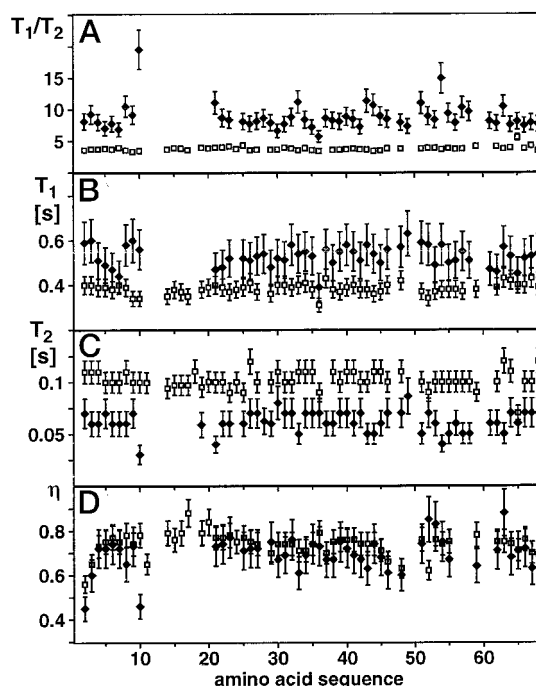


FIG. 6. Relaxation times and steady-state  $^{15}N\{^1H\}$ -NOEs measured for the backbone amide nitrogen atoms of *apo*-CopZ ( $\square$ ) and Cu(I)-CopZ ( $\blacklozenge$ ). a,  $T_1/T_2$  recorded at a  $^{15}N$  frequency of 50.7 MHz; b, longitudinal relaxation time  $T_1$ ; c, transverse relaxation time  $T_2$ ; d,  $^{15}N\{^1H\}$ -NOEs recorded at a  $^{15}N$ -frequency of 60.8 MHz. For Cu(I)-CopZ no measurements were obtained for the residues 11–20 (see text).

Because traces of paramagnetic Cu(II) could strongly influence the results of the relaxation measurements, the NMR samples were checked for the presence of paramagnetic oxidized copper using EPR. No EPR signals above the background from the sample tube were detected in the Cu(I)-CopZ solutions used for the NMR studies (data not shown).

*Dynamic Light Scattering Studies of CopZ Aggregation in the Presence and Absence of Cu(I)*—Dynamic light scattering of *apo*-CopZ measured at 293 K yielded a hydrodynamic radius of  $19.2 \pm 0.8$  Å for a spherical particle in a solvent with the viscosity of water. The corresponding value for Cu(I)-CopZ was found to be  $25.9 \pm 1.8$  Å. The increase of  $35 \pm 15\%$  lies within the range that could be expected from dimerization (37, 38). The experimental data showed sizeable variability, corresponding to confidence intervals of the order of  $\pm 7\%$ , which probably reflects a wide distribution of sizes and/or shapes of the Cu(I)-CopZ aggregates.

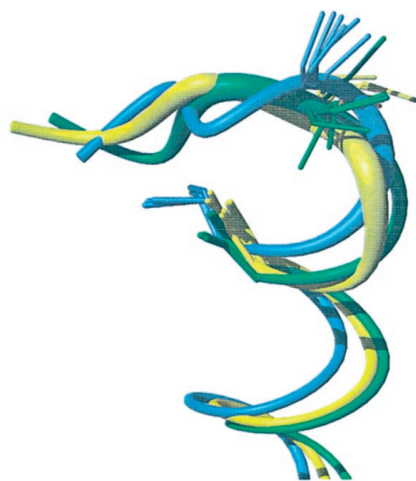


FIG. 7. Comparison of the metal-binding sites of *apo-CopZ* (yellow), *apo-MerP* (blue), and *apo-mbd4* (green), including the residues that correspond to the loop between  $\beta_1$  and  $\alpha_1$  and the first two turns of  $\alpha_1$  in *apo-CopZ*. The six best conformers of each protein are represented by the mean of the backbone coordinates and by a superposition of the two Cys side chain arrangements in the six conformers.

#### DISCUSSION

Unlike other cupro-proteins, CopZ binds copper as a substrate that can be delivered to target proteins, rather than as a cofactor. The solution structure of CopZ and the observed effects of metal binding upon it now add to our understanding of such intracellular routing of copper, especially when compared with corresponding features of other Cu(I) proteins. The  $\beta\alpha\beta\alpha\beta$ -fold of *apo-CopZ* is similar to those observed for the fourth metal-binding domain MNKv4 of the Menkes ATPase, and the bacterial mercury chaperone MerP (19, 20), but there are major differences between CopZ and MNKv4 or MerP in the loop between the first  $\alpha$  helix and the first  $\beta$  strand, which contains the CXXC metal binding motif in all these proteins. The relative orientations of the cysteines, Cys-11 and Cys-14, in *apo-CopZ* are such that they could not coordinate Cu(I) without major side chain and possibly backbone structural rearrangement. This is not the case in MNKv4, but resembles the situation in MerP, where the structure of the loop in the *apo*-protein (Fig. 7) was altered upon binding of mercury to allow a nearly linear S–Hg(II)–S arrangement, which is the preferred coordination of Hg(II) (19).

In Cu(I)-CopZ the metal binding loop is so extensively affected by Cu(I) interactions that most of the NMR signals expected for the amino acid residues 11 to 20 could not be observed. Nuclear magnetic relaxation data showed an increase in correlation time due to an increase in molecular mass for Cu(I)-CopZ when compared with *apo-CopZ*, which is indicative of self-aggregation. The presence of aggregated protein was further corroborated by light scattering measurements. From experiments on the transfer of Cu(I) from CopZ to CopY (8) we know that the stoichiometry of Cu:CopZ is 1:1. If we assume that the observed aggregation corresponds to dimer formation, such dimers would thus contain two copper ions. Cu(I)-CopZ-Cu(I)-CopZ interactions in a dimeric species might thus contribute to the modified NMR features in the metal binding loop region. No sizeable chemical shift changes in other parts of the molecule were observed except for residues Glu-46 and Gly-62, which are located in the two linker peptides with the helix  $\alpha_2$ . Gly-62 is in spatial proximity to the binding loop. Thus there is no evidence for extensive contacts between CopZ molecules in molecular regions distant to residues 10 to 20. In as far as they could be measured, the chemical shifts of the two

CopZ moieties in the presumed dimer are equivalent, which would be compatible with the copper-binding residues of both CopZ molecules in a Cu(I)-CopZ dimer being in spatial proximity. The fact that most NMR signals in the copper-binding region of CopZ could not be found in Cu(I)-CopZ would further be compatible with a dynamic mode of interaction between two or more Cu(I)-CopZ molecules. Dimerization would most likely involve the formation of intermolecular thiolate bridges, leading to three-coordinated copper(I).

In MNKv4, Ag<sup>+</sup> instead of the implicated natural copper substrate was used to solve the metal-bound structure. Ag(I) preferentially forms bidentate complexes, and MNKv4 could apparently accommodate Ag(I) without major rearrangements (20). However, purified MNKv2 of the same enzyme was demonstrated to bind Cu(I) with a stoichiometry of 1 copper/domain, and circular dichroism studies suggested that the binding or loss of copper did not cause substantial changes to the secondary structure of the protein (39). By extended x-ray absorption fine structure techniques, it was shown that MNKv2-bound Cu(I) is in a mixed coordination with two and three ligands, whereas Ag(I) is bound with two ligands, with all ligands being sulfur. The identity of the third ligand in the Cu(I)-MNKv2 complex remains unknown, but the presence of a copper-copper scatter peak in the spectral data suggested Cu(I)-thiolate bridge formation between different Cu(I)-mbd2 molecules (39, 40). Extended x-ray absorption fine structure analysis of Cu(I)-Atx1, which is the yeast homologue of CopZ, had similarly indicated that copper(I) is bound in a mixed two- and three-coordinated fashion (41). This could be because of a buffer thiolate forming the third ligand, but thiolate bridge formation with another Atx1 molecule could not be excluded.

In the Cu(I)-CopZ structure, we rule out an involvement of Met-9 as a third intramolecular copper ligand, because the chemical shifts of both C<sup>ε</sup> and H<sup>ε</sup> did not change markedly upon addition of Cu(I). In yeast Atx1, mutation of the corresponding methionine to leucine did not affect the activity of the chaperone *in vivo*, supporting that this residue has no role in metal binding (41). The fourth potential intramolecular sulfur ligand in CopZ, Cys-55, seems not to be involved in copper binding either, because the H<sup>γ</sup> NMR lines of Cys-55 were observable in the spectra of both *apo-CopZ* and Cu(I)-CopZ, and there is no corresponding cysteine in other CopZ-like chaperones. An intermolecular thiolate-bridge in the observed dimerization of Cu(I)-CopZ would explain the origin of a third sulfur ligand. We think that *in vivo* the third ligand could be glutathione, given the high concentration of glutathione in cells (42) and the known tendency of glutathione to bind Cu(I) (43).

If copper(I) in CopZ adopts a three-coordinate structure, a copper exchange mechanism could be envisioned as follows. When Cu(I)-CopZ docks on a recipient molecule, the third copper ligand (*e.g.* a second CopZ molecule or a small molecule) could be replaced by a sulfur ligand of the recipient molecule (41). Next, copper would be complexed by a second ligand of the recipient molecule, with concomitant release of a CopZ ligand. Finally, copper would be released from CopZ and remain bound to the recipient molecule.

We have recently shown *in vitro* that Cu(I)-CopZ donates two Cu(I)-ions to the copper-responsive repressor CopY of *E. hirae*. Copper transfer displaced zinc(II) from CopY, which released the repressor from the DNA-binding site. The transfer was specific for CopZ, as Cu(I)-mbd2 was unable to donate copper to CopY (8). This suggests that specific protein-protein interactions between CopZ and the CopY repressor might be involved in copper transfer. In this light, the distribution of charged residues on the surface of CopZ is of interest. The clustering of seven lysine residues in the  $\beta$ -strands 2 and 3, in positions 29,

30, 32, 36, 37, 39, and 43, generates a positively charged face on the molecule (Fig. 1d). On the opposite surface of CopZ a clustering of the 7 acidic residues Glu-3, Glu-66, Glu-60, Glu-53, Glu-46, Asp-45, and the C-terminal carboxylate group generates a negatively charged surface area (Fig. 1c). These surface features are likely to play a role in molecular recognition for specific protein-protein interactions in the course of copper exchange. An example for such recognition sites is a clustering of basic residues on cytochrome *c* that interacts electrostatically with negatively charged residues on cytochrome *c* oxidase or peroxidase (44, 45). It is tempting to speculate that one of the charged faces of CopZ is required to interact with a copper donor, and the other one supports recognition of a copper acceptor, such as CopY. In this context it seems worth mentioning that the electrostatic potential on the surface of MerP is different from that of CopZ and that the function of this protein is also quite different. MerP scavenges mercury in the periplasmic space to donate it to MerT, which transports it through the membrane into the cytoplasmic space (17).

In the absence of direct information on how CopZ interacts with other proteins, knowledge of the structure of CopZ provides important clues with respect to possible interaction mechanisms for efficient copper chaperoning. In conjunction with the *in vitro* system for the measurement of copper transfer from CopZ to CopY, mechanistic models can now specifically be addressed.

**Acknowledgments**—We thank Thomas Weber and Sandra Krebs-Stoll for preparation and biochemical characterization of CopZ, and Charles Dameron and Peter Güntert for helpful discussions. We are obliged to Josef Granwehr and Paul Schosseler from the Laboratorium für Physikalische Chemie of the ETH in Zürich for recording and discussing the EPR spectra. We express gratitude to Stefan Umhau from the Institute of Biophysics of the University of Constance for the light scattering measurements.

**Note Added in Proof**—After submission of the present report, the structure of the oxidized *apo*-form and the Hg-form of Atx1, the yeast homologue of CopZ, was published (Rosenzweig, A. C., Huffman, D. L., Hou, M. Y., Wernimont, A. K., Pufahl, R. A., and O'Halloran, T. V. (1999) *Structure* **7**, 605–617).

## REFERENCES

- Lutsenko, S., and Kaplan, J. H. (1995) *Biochemistry* **34**, 15607–15613
- Soloz, M., and Vulpe, C. (1996) *Trends Biochem. Sci.* **21**, 237–241
- Lin, S. J., and Culotta, V. C. (1995) *Proc. Natl. Acad. Sci. U. S. A.* **92**, 3784–3788
- Lin, S. J., Pufahl, R. A., Dancis, A., O'Halloran, T. V., and Culotta, V. C. (1997) *J. Biol. Chem.* **272**, 9215–9220
- Odermatt, A., Suter, H., Krapf, R., and Soloz, M. (1992) *Ann. N. Y. Acad. Sci.* **671**, 484–486
- Odermatt, A., Suter, H., Krapf, R., and Soloz, M. (1993) *J. Biol. Chem.* **268**, 12775–12779
- Odermatt, A., and Soloz, M. (1995) *J. Biol. Chem.* **270**, 4349–4354
- Cobine, P., Wickramasinghe, W. A., Harrison, M. D., Weber, T., Soloz, M., and Dameron, C. T. (1999) *FEBS Lett.* **445**, 27–30
- Himelblau, E., Mira, H., Lin, S. J., Cizewski Culotta, V., Penarrubia, L., and Amasino, R. M. (1998) *Plant Physiol.* **117**, 1227–1234
- Klomp, L. W., Lin, S. J., Yuan, D. S., Klausner, R. D., Culotta, V. C., and Gitlin, J. D. (1997) *J. Biol. Chem.* **272**, 9221–9226
- Silver, S., and Phung, L. T. (1996) *Annu. Rev. Microbiol.* **50**, 753–789
- Fu, D., Beeler, T. J., and Dunn, T. M. (1995) *Yeast* **11**, 283–292
- Griffin, H., Foster, T. J., Silver, S., and Misra, T. K. (1992) *Proc. Natl. Acad. Sci. U. S. A.* **84**, 3112–3116
- Kägi, J. H., and Schaffer, A. (1988) *Biochemistry* **27**, 8509–8515
- Silver, S., Nucifora, G., and Phung, L. T. (1993) *Mol. Microbiol.* **10**, 7–12
- Soloz, M. (1998) in *Ion Pumps* (Andersen, J. P., ed) pp. 167–203, JAI Press Ltd., London
- Morby, A. P., Hobman, J. L., and Brown, N. L. (1995) *Mol. Microbiol.* **17**, 25–35
- Sahlman, L., and Skarfstad, E. G. (1993) *Biochem. Biophys. Res. Commun.* **196**, 583–588
- Steele, R. A., and Opella, S. J. (1997) *Biochemistry* **36**, 6885–6895
- Gitschier, J., Moffat, B., Reilly, D., Wood, W. L., and Fairbrother, W. J. (1998) *Nat. Struct. Biol.* **5**, 47–54
- Strausak, D., and Soloz, M. (1997) *J. Biol. Chem.* **272**, 8932–8936
- Bartels, C., Xia, T., Billeter, M., Güntert, P., and Wüthrich, K. (1995) *J. Biomol. NMR* **6**, 1–10
- Wüthrich, K. (1986) *NMR of Proteins and Nucleic Acids*, John Wiley & Sons, Inc., New York
- Piantini, U., Sørensen, O. W., and Ernst, R. R. (1982) *J. Am. Chem. Soc.* **104**, 6800–6801
- Müller, N., Ernst, R. R., and Wüthrich, K. (1986) *J. Am. Chem. Soc.* **108**, 6482–6492
- Szyperki, T., Güntert, P., Otting, G., and Wüthrich, K. (1992) *J. Magn. Reson.* **99**, 552–560
- Düx, P., Whitehead, B., Boelens, R., Kaptein, R., and Vuister, G. W. (1997) *J. Biomol. NMR* **10**, 301–306
- Farrow, N. A., Muhandiram, R., Singer, A. U., Pascal, S. M., Kay, C. M., Gish, G., Shoelson, S. E., Pawson, T., Forman-Kay, J. D., and Kay, L. E. (1994) *Biochemistry* **33**, 5984–6003
- Lounila, J., Oikarinen, K., Ingman, P., and Jokisaari, J. (1996) *J. Magn. Reson. A* **118**, 50–54
- Güntert, P., Braun, W., and Wüthrich, K. (1991) *J. Mol. Biol.* **217**, 517–530
- Güntert, P., Mumenthaler, C., and Wüthrich, K. (1997) *J. Mol. Biol.* **273**, 283–298
- Güntert, P., Billeter, M., Ohlenschläger, O., Brown, L. R., and Wüthrich, K. (1998) *J. Biomol. NMR* **12**, 543–548
- Luginbühl, P., Güntert, P., Billeter, M., and Wüthrich, K. (1996) *J. Biomol. NMR* **8**, 136–146
- Hemmerich, P., and Sigwart, C. (1963) *Experientia* **19**, 488–489
- Laskowski, R. A., MacArthur, M. W., Moss, D. S., and Thornton, J. M. (1993) *J. Appl. Crystallogr.* **26**, 283–291
- Kay, L. E., Torchia, D. A., and Bax, A. (1989) *Biochemistry* **28**, 8972–8979
- Schurtenberger, P., and Newman, M. E. (1993) in *Environmental Particles* (Buffle, J., and van Leeuwen, H. P., eds) pp. 37–115, Lewis Publishers, Inc., Boca Raton, FL
- Perrin, F. (1936) *J. Phys. Radium* **7**, 1–11
- Harrison, M. D., Meier, S., and Dameron, C. T. (1999) *Biochim. Biophys. Acta* **1453**, 254–260
- Cobine, P., Harrison, M. D., and Dameron, C. T. (1999) *Adv. Exp. Med. Biol.* **448**, 153–164
- Pufahl, R. A., Singer, C. P., Peariso, K. L., Lin, S., Schmidt, P. J., Fahrni, C. J., Culotta, V. C., and Penner-Hahn, J. E. (1997) *Science* **278**, 853–856
- Tietze, F. (1969) *Anal. Biochem.* **27**, 502–522
- Corazza, A., Harvey, I., and Sadler, P. J. (1996) *Eur. J. Biochem.* **236**, 697–705
- Hildebrandt, P., Vanhecke, F., Buse, G., Soulimane, T., and Mauk, A. G. (1993) *Biochemistry* **32**, 10912–10922
- Hazzard, J. T., McLendon, G., Cusanovich, M. A., Das, G., Sherman, F., and Tollin, G. (1988) *Biochemistry* **27**, 4445–4451
- Koradi, R., Billeter, M., and Wüthrich, K. (1996) *J. Mol. Graph.* **14**, 51–55